Research Article

Mechanism and Evolution Control of Wide Coal Pillar Bursts in Multithick Key Strata

Wenhao Guo [ID],[1] Anye Cao [ID],[1,2] Chengchun Xue [ID],[1] Yang Hu,[1] Songwei Wang,[1] and Qian Zhao[3]

[1]*School of Mines, China University of Mining and Technology, Xuzhou, Jiangsu 221116, China*
[2]*Jiangsu Engineering Laboratory of Mine Earthquake Monitoring and Prevention, China University of Mining and Technology, Xuzhou 221116, China*
[3]*Menkeqing Coal Mine, Zhongtian Hechuang Energy Co. Ltd, Ordos 017000, China*

Correspondence should be addressed to Anye Cao; caoanye@163.com

Coal mine pillar burst frequently occurs in Western China, which seriously restricts safe production. This paper takes the 35 m coal pillar of the 3102 working face of MKQ coal mine as the engineering background. The mechanism and evolution control of pillar bursts in multithick key strata are studied using field investigation, theoretical analysis, and numerical simulation. The mechanism of dynamic and static stress-induced pillar bursts was revealed combining the "O-X" broken features for key strata and numerical simulation of pillar stress evolution. A prevention scheme is put forward for strata presplit blasting and adjusting coal pillar width to minimize the dynamic and static stresses. The results demonstrate the following. (1) In the multithick strata, the first and second near-field subkey strata have perpendicular "O-X" broken features, whereas the third far-field subkey has parallel "O-X" broken features. The working face has three kinds of periodic weighting phenomena: long, medium, and short. (2) The simulated vertical stress curve of 35 m coal pillar goes through three states: two-peak, asymmetric trapezoidal and symmetrical trapezoidal shape with the different advancing position of working face. The stress concentration is extensively promoting a high-risk area for rock burst. (3) The coal pillar burst was induced by the superposition of energy released by the key strata breaking and the elastic energy accumulated in the wide coal pillar. (4) The monitoring data showed that the long, medium, and short periodic weighting steps of multithick key strata are 141.6 m, 43.2–49.6 m, and 17.6–27.2 m, respectively. The microseismic events energy, frequency, and stress of hydraulic support increment are the highest during the long periodic weighting, and the spatial distribution of microseismic events coincides with the stress concentration area. The theoretical analysis is confirmed with the field practice.

1. Introduction

The mining depth of China's coal mines often exceeds 600–800 m, so rock burst has become one of the major disasters restricting coal mines' safe and efficient production under high in situ stress and complex geological conditions [1]. Due to the influence of inappropriate coal pillars and thick strata, pillar bursts, as a type of rock burst, frequently occur in China's central and western coal mines [2]. Under the disturbance of multiple abutment pressures, the stress of coal pillars around the goaf was high, especially when there were multithick key strata in the roof. The large-scale breaking or caving of key strata induced strong mine tremor, rock burst, and other dynamic disasters [3]. For example, on March 27, 2014, the air-return roadway of 21032 working faces of Qianqiu Coal Mine was driving in the isolated coal pillar, a pillar burst occurred that resulted in six deaths [4]. On November 11, 2017, when the 702 working face of Hongyangsan Coal Mine advanced to 1740 m, a rock burst occurred in the air-return roadway, and the 32 m coal pillar slid into the middle of the working face by 1–3 m, resulting in 10 deaths and one injury [5].

Some scholars have studied the coal pillar burst mechanism and found that pillar burst was related to its static stress status and is affected by dynamic stress from the roof [6, 7]. Wang et al. [3] and Maleki Hamid [8] found that the "roof-pillar" systems geometric parameters and mechanical properties directly impacted the stability of the coal pillar. The dynamic stress generated by roof breaking was transferred to the coal pillars, causing pillar burst. Bo-Hyun Kim et al. [9] revealed the relationship between coal pillar burst and surrounding rock stress through a Utah coal mine's field analysis and laboratory experiment. Using numerical simulation, Yang et al. [10] and Newman and Christopher et al. [11] showed that the superposition of the abutment pressure from two adjacent goaves further enhanced the coal pillar's stress regime. Zhu. et al. [12]. proposed the method to estimate the static and dynamic stress on isolated coal pillars and constructed the pre-assessment system of an isolated working face's rock burst risk before mining. Li et al. [13]. established the mechanical model of the fault-pillar and observed that the smaller the pillar's width, the easier the roof was to rotate, and the pillar stress increased with the decrease of its width and the increase of the overhanging length of the roof. The above research results showed that the impact of the roof on coal pillars was complex, including roof stiffness, breaking form, and goaf. Furthermore, the coal pillar burst mechanism and characteristics differed with different roof structures, hindering the monitoring from preventing coal pillar burst.

The broken characteristics of multikey strata during coal mining also had an impact on coal pillars burst. Han et al. [14] found that the roof strata in goaf were broken from bottom to top, causing multiple disturbances to mining stope. The thicker and more extensive the overhanging roof strata were, the more significant the disruption was. Similarly, through the analysis of hydraulic support resistance, Liu et al. [15] found that the breaking form and the order of the multithick key strata influenced the mine pressure behavior, especially with the multithick strata synchronous caving. Zhao et al. [16] found that the broken characteristics of the key strata changed under different adjacent goaf conditions by analyzing the roof structure of Hongqinghe 3–1103 working face, which brought further disturbances to the coal pillar. Zhu et al. [17] studied the mining of shallow buried ultraclose seams and found that breaking the main key layer released the highest energy and posed the highest risk.

The current research results showed that the abutment pressure of goaf and the breaking dynamic stress of key strata were the leading causes of coal pillar burst. However, there was rarely any research on coal pillar bursts combined with multilayer thick key strata. Therefore, they are aimed at the characteristics for multithick key strata caving, stress evolution in wide coal pillar, and mining stope in MKQ coal mine. This paper discusses the mechanism and the development of wide coal pillars burst with multithick key strata and provides the corresponding basis for preventing similar coal bursts.

2. Cases of Coal Pillar Burst

2.1. Production and Geological Conditions of Working Face. MKQ coal mine is the first rock burst mine in the Hogilt mining area of Ordos, Inner Mongolia. Its buried depth is more than 600 m and has multilayer thick roof (the roof within 200 m above the coal seam contains multiple layers of 10–40 m thick strata), and the width of the coal pillar is 25–35 m, which are representative in Hujierte mining area. According to incomplete statistics, during the advancing of 3102 working faces (LW3102) in the MKQ coal mine from August 10, 2017, to April 8, 2018, the coal pillar adjacent to the goaf experienced 16 pillar bursts of different degrees. In addition, similar pillar bursts occurred in the nearby Muduchaideng coal mine, Hulusu coal mine, and so on. The rock burst of these three mines is located in the gob-side roadway, and the distribution range is about 0–300 m ahead of the working face. The rock burst basically occurs in periodic weighting, accompanied by microseismic events with energy between 10^4 and 10^6 J, and the damage length is between 20 and 200 m. At the same time, it will generally have the phenomena of coal pillar failure, roof subsidence, and floor heave. Therefore, it is significant to study the mechanism and the evolution of pillar burst with multithick roofs for rock burst prevention in the Hogilt mining area.

The second working face of the MKQ coal mine is LW3102, located in the southern boundary of the No.11 working district, with a strike length of 5540 m and a dip length of 300 m. The south side of the LW3102 was the boundary of the mine. The north side was a 3–1 coal air-return roadway. The west side was 3101 goafs, and the width of the coal pillar was 35 m. The mining depth of LW3102 is 690 m–700 m. The 3–1 coal seams were mined according to fully mechanized mining. The thickness of 3–1 coal seam was 4.35–5.47 m, with an average of 5.1 m, as shown in Figure 1; dip angle is 1–4°, with an average of 2°. Figure 2 gives the layout of LW3102.

According to the histogram of 602 boreholes in LW3102 shown in Figure 1, seven thick strata (thickness is more than 10 m) within 200 m above 3–1 coal seam. Therefore, it was prudent to first identify the key strata distribution in the multilayer thick strata group [18]. Firstly, we assume that the key stratum b controls the local or all strata activities overlying it, and its total load can be obtained by superposition of its control strata load through beam theory, as shown in (1). Moreover, when a load from stratum a above stratum b was less than that of stratum a-1, it indicated that stratum a no longer needed the support of stratum b, then the highest stratum controlled by key stratum b was stratum a-1, and stratum a was a new key stratum, as shown in (2).

The bearing relationship of the roof from top to bottom had the following relationship:

$$(q_a)_b = E_b h_b^3 \frac{\sum_{i=b}^{a} \gamma_i h_i}{\sum_{i=b}^{a} \gamma_i h_i^3},\tag{1}$$

where $(q_a)_b$ is a load of stratum a to stratum b; a, b, and i are the serial numbers of roof strata; $E_b\,{}_h^b$ is the elastic modulus

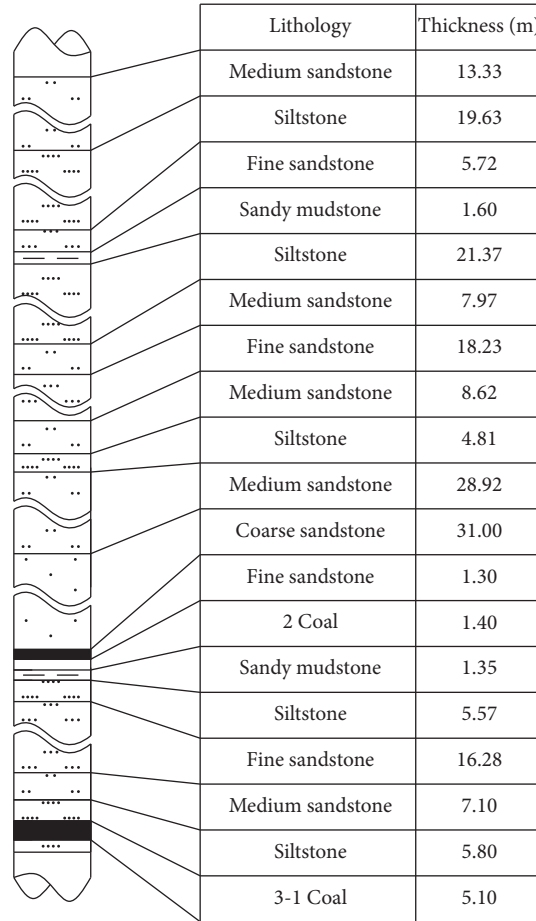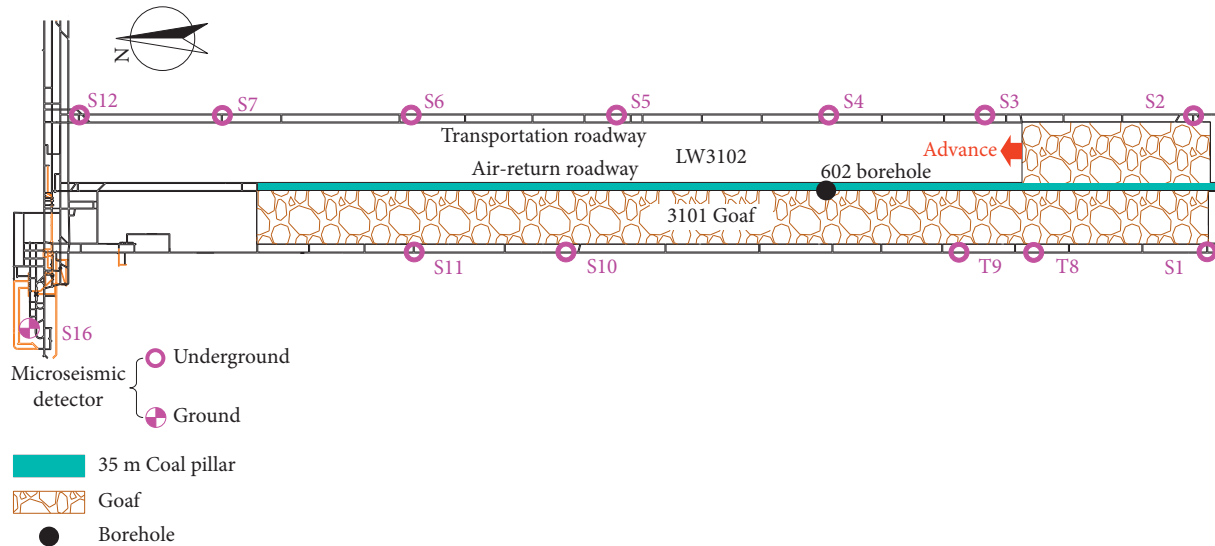| Lithology	Thickness (m)
Medium sandstone	13.33
Siltstone	19.63
Fine sandstone	5.72
Sandy mudstone	1.60
Siltstone	21.37
Medium sandstone	7.97
Fine sandstone	18.23
Medium sandstone	8.62
Siltstone	4.81
Medium sandstone	28.92
Coarse sandstone	31.00
Fine sandstone	1.30
2 Coal	1.40
Sandy mudstone	1.35
Siltstone	5.57
Fine sandstone	16.28
Medium sandstone	7.10
Siltstone	5.80
3-1 Coal	5.10

FIGURE 1: 602 boreholes.

FIGURE 2: Geological conditions and layout of a microseismic monitoring system of LW3102.

and thickness of the stratum b; E_i, h_i, and γ_i are elastic modulus, thickness, and bulk density of the stratum i.

The discriminant equation for the stratum a as the key stratum is

$$(q_a)_b < (q_{a-1})_b. \tag{2}$$

Therefore, according to the key layer theory [19], No.1 fine sandstone, No.2 coarse sandstone, and No.5 siltstone

within 200 m above 3–1 coal seam were subkey strata (SKS) as shown in Table 1.

ARAMIS-M/E microseismic monitoring system was installed in MKQ coal mine to monitor the time of events accurately, location, energy, and other data of microseismic (MS) events [20]. Twelve MS detectors are installed underground around LW3101 and LW3012. In addition, a single sensor was installed on the ground near the shaft, as shown in Figure 2. Furthermore, LW3102 was equipped with a hydraulic stress monitoring station for every 18 hydraulic support to record roof movement, and a total of 10 monitoring stations were installed with a monitoring frequency of 1 time per minute, as shown in Figure 3.

2.2. Characteristics of Coal Pillar Burst. During the mining of LW3102, many different levels of rock burst occurred. Table 2 lists the occurrence time, location, and damage length of the six representative rock burst, and two cases of "3.3" and "4.8" rock bursts that occurred after installing the MS monitoring system on January 4, 2018, were analyzed.

In "3.3" rock burst, at 17 : 11 : 51 on March 3, 2018, a rock burst occurred in LW3102 with source energy of 6.4×10^6 J. The source location of MS was 153 m ahead of the LW3102, and the duration was about 3000 ms. Figure 4(a) shows the MS waves and source location. Some wooden buttresses collapsed in the area of 0–180 m ahead of the working face; the floor heave was severe in 120–180 m, and the maximum floor heave was more than 1 m.

In "4.8" rock burst, at 12 : 59 : 51 on April 8, 2018, a rock burst occurred in LW3102 with source energy of 3.0×10^7 J, and the source location of MS was 150 m ahead of the working face. When the MS event occurred, there was a tremor on the ground, and China Seismic Network Center had detected that the corresponding mine earthquake had a magnitude of 2.5. Figure 4(b) shows the MS waves and source location. At the tail of the LW3102, the 172–175 hydraulic support was buried. The bolts and metal mesh were torn in the area 0–114 m ahead of the working face, and some hydraulic props and wooden buttresses got damaged in the 114–300 m area.

The six rock burst space locations were in 35 m coal pillars near goaves, and all occurred during periodic weighting of LW3102. Therefore, according to rock burst's occurrence space and time and the strata distribution above 3–1 coal seam, 35 m coal pillar burst was closely related to multithick key strata.

3. Mechanism of Wide Coal Pillar Burst with Multithick Key Strata

3.1. Broken Features of Multithick Key Strata. The broken features of the key strata, including the overhanging area and movement of blocks, differ significantly due to the width of the working face, the thickness of strata, rock fracture angle, and the distance to the coal seam [18].

As shown in Figure 5, under the influence of rock stratum fracture angle α, for working face with fixed-width a, the overhang length l_2 of the key strata decreases with the

increase of distance H_i from the coal seam, and the weighting step l_1 of the key strata will be different under a different l_2. Combined with the "O-X" theory of key strata fracture, the strata will produce "O" fracture on the long side and "X" fracture on the short side. Therefore, the "O-X" breaking characteristics need further analysis with the length of l_1 and l_2 affected by H_i.

In Figure 5, H_i is the distance between the key strata and coal seam and a is the width of the working face. Assuming that the rock fracture angle is α, the overhanging width l_2 of the key strata is determined using

$$l_2 = a - \frac{(2H_i)}{\tan \alpha}. \tag{3}$$

Combined with the spatial distance of 3101 goaves, the key strata of LW3102 were regarded as a plate supported simply on two neighboring sides and clamped support on the other two adjacent sides. Therefore, the relationship between the weighting step l_1 of the key strata was analyzed using thin-plate theory [21]:

$$l_1 = \frac{2H_i}{1 - \mu^2} \bullet \sqrt{\frac{\sigma_s}{3q} \bullet \frac{1 + \lambda^4}{1 + \mu \lambda^2}}, \tag{4}$$

where μ and σ_s are Poisson's ratio and tensile strength of key strata; q is a superposition of the self-weight and the upper loads from the key strata; λ is the geometric coefficient of the mining area, which is the ratio of the first weighting step and the width of the working face.

Following (4), combined with the overhanging width l_2, working face width a, and weighting step l_1, the broken features of the key strata are classified as follows. (1) When the overhanging width is longer than the weighting step ($l_2 > l_1$), perpendicular "O-X" breaking of the key strata occur. (2) When the overhanging width is shorter than the weighting step ($l_2 < l_1$), parallel "O-X" cracking of the key strata occurs, as shown in Figure 5.

In addition, when perpendicular "O-X" breaking occurred in the key strata, it was close to the coal seam as in the near-field key strata. At this time, the second block was adjacent to the boundary of the mining area and caused the coal pillar stress to rise after the rotary sinking. When parallel "O-X" breaking occurred in the key strata, it is far from the coal seam as the far-field key strata. The main block is adjacent to the boundary of the mining area, and the rotary sinking caused the stress to rise in the coal pillar.

Combined with the 602 borehole information shown in Figure 1, the key strata data in Table 1, and equations (3) and (4), the broken features of the multikey strata in LW3102 are delineated and shown in Table 3.

Large-scale breaking of the key strata induces coal pillar bursts [13, 22]. The key strata's breaking, rotation, and sinking transfer its gravitational load and the bearing strata load to the coal pillar, which causes an increment of pillar stress. The energy released by the key strata breaking is superimposed on the elastic energy accumulated in the coal pillar, thus inducing the coal pillar to burst.

TABLE 1: Strata distribution above 3–1 coal seam.

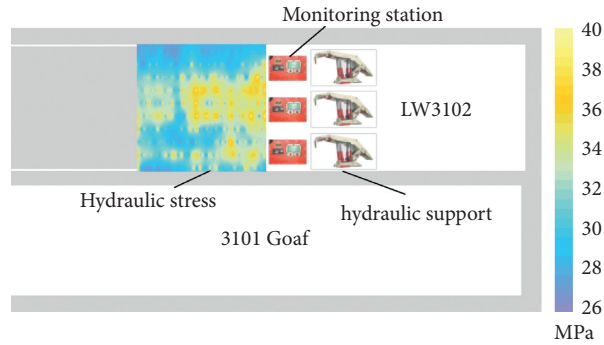| No.	Lithology	Thickness (m)	Distance to coal seam (m)	Discrimination
1	Fine sandstone	16.3	12.9	SKS1
2	Coarse sandstone	31.0	38.8	SKS2
3	Medium sandstone	28.9	69.8	
4	Fine sandstone	18.2	112.2	
5	Siltstone	21.4	138.4	SKS2
6	Siltstone	19.6	167.0	
7	Medium sandstone	11.4	186.7	

FIGURE 3: Hydraulic support monitoring system in LW3102.

TABLE 2: Statistical of representative rock burst of LW3102.

No.	Date	Energy (J)	Roof condition	Location	Damage length (m)	Damages of air-return roadway
1	2017.11.26	—	Periodic weighting	Coal pillar near goaf	25	The roof coal caved at the side of the coal pillar; the length, width, and height of the damaged area were 18 m, 1.5 m, and 0.6 m, respectively; in addition, the bolts and metal mesh failed
2	2017.12.13	—	Periodic weighting	Coal pillar near goaf	25	The roof subsidence was about 0.3–0.5 m; the floor heave was about 0.3–0.6 m; pillar walls were spalled; some hydraulic prop toppled
3	2017.12.25	—	Periodic weighting	Coal pillar near goaf	38	The roadway roof at the coal pillar side was inclined in the area 0–38 m ahead of LW3102; some wooden buttresses got damaged; tremors were felt
4	2018.1.26	—	Periodic weighting	Coal pillar near goaf	25	The roof subsidence was about 0.3–0.5 m; the floor heave was about 0.3–0.6 m, two walls spalled, and some hydraulic prop toppled in the 25 m ahead of LW3102
5	2018.3.3	6.4×10^6	Periodic weighting	Coal pillar near goaf	180	The floor heave was 1 m, with some hydraulic prop and wooden buttresses damaged in the 0–180 m ahead of LW3102; the ventilation of the air-return roadway was reduced from 2100 m^3/min to 1820 m^3/min due to deformation
6	2018.4.8	3×10^7	Periodic weighting	Coal pillar near goaf	300	The floor heave was about 1.2–1.3 m; the bolts and metal mesh were torn in the area 0–114 m ahead of LW3102; coal burst out in the area 45 m ahead LW3102

As shown in Table 3, the broken features of SKS1 and SKS2 near-field key strata in LW3102 are perpendicular "O-X," with shorter weighting step, smaller overhanging area, and less breaking energy compared with SKS3. The secondary block rotating and sinking caused the coal pillar stress to rise. On the other hand, SKS3 was a far-field key stratum, the broken features were parallel "O-X," with long weighting steps, and the overhanging area was four and twice that of SKS1 and SKS2, respectively. Hence, the breaking energy was significantly high. In addition, the main blocks of SKS3 acted on the coal pillar, and its area was more

significant than the second block of SKS1 and SKS2, and the stress of the coal pillar rose significantly. Therefore, according to the above analysis, the LW3102 showed three periodic weighting phenomena: long, medium, and short, corresponding to SKS3, SKS2, and SKS1, respectively.

3.2. Numerical Simulation of Stress Evolution in Wide Coal Pillars. The stress distribution of coal pillars differed with different coal pillar widths and adjacent goaf [23]. According to the actual geological conditions and the stress distribution
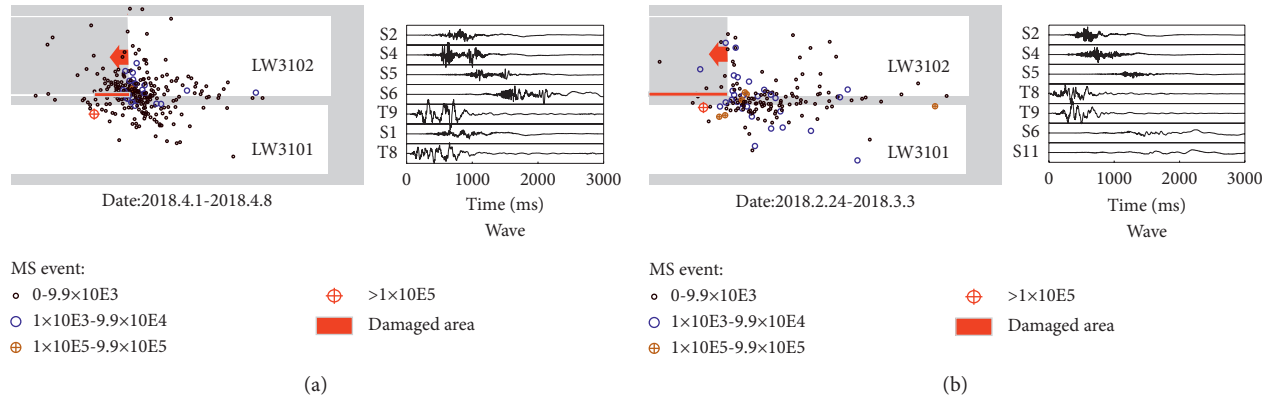
FIGURE 4: Location of MS event and damage area. (a) "3.3" rock burst. (b) "4.8" rock burst.
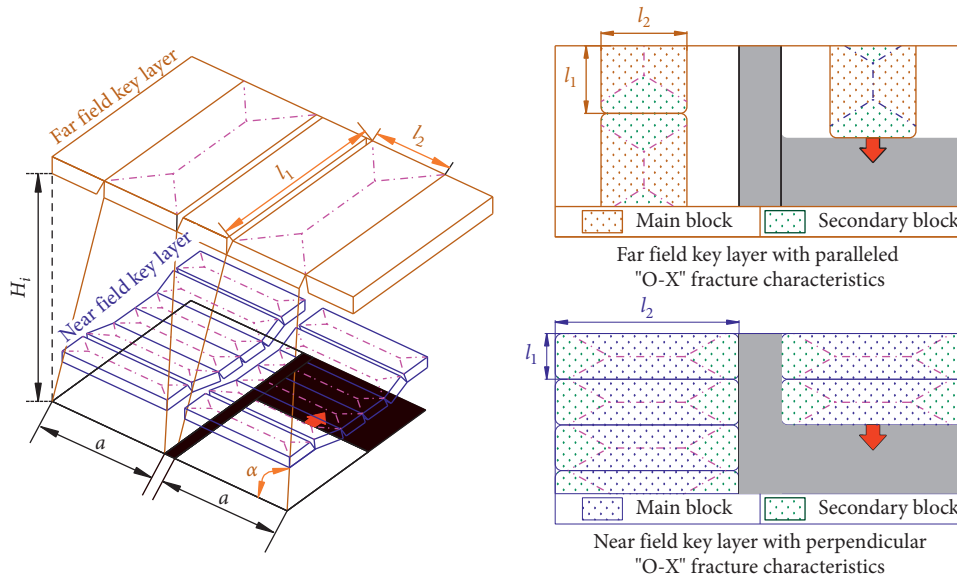

FIGURE 5: "O-X" broken features model of the different key strata.

of wide coal pillars in LW3102, the FLAC3D numerical simulation model was established. Its length, width, and height were 1000 m, 800 m, and 300 m, respectively. Constant stress (12 MPa) replaced the nonsimulated strata that overlay the coal seam. The model's base was a fixed boundary, while the other surfaces, except the top, were rolling support boundaries. Mohr–Coulomb strength criterion was adopted in the simulation model [24]. According to the rock mechanics test results of the MKQ coal mine and adjacent mines, the physical and mechanical parameters of coal and rock in the model are shown in Table 4.

We simulated the stress distribution in the 35 m coal pillar when it was 180 m, 100 m, and 20 m ahead of LW3102 and 20 m, 100 m, and 180 m behind LW3102, as shown in Figures 6 and 7. There are three stress states of wide coal pillars with different distances from LW3102. (1) When the wide coal pillar was located in position I-I (180 m ahead of LW3102), only 3101 goaves were around. Affected by the sinking and subsidence of overhanging strata in 3101 goaves,

the vertical stress on the goaf side of the coal pillar increased to 29.62 MPa, and the vertical stress on the roadway side of the coal pillar increased to 25.96 MPa, which was smaller than the peak vertical stress on the goaf side. The vertical stress in the center of the coal pillar superimposed the abutment pressure of roadway and goaf, which is larger than the in situ stress but less than the peak stress. At this time, the vertical stress curve of the coal pillar is a two-peak shape. (2) When the wide coal pillar located in positions II-II and III-III (100 m, 20 m ahead of LW3102, respectively), compared with the position I–I, the coal pillar is gradually affected by the abutment pressure of goaf of LW3102, and the peak stress of the coal pillar further increased to 35.06 MPa and 45.08 MPa, respectively. The vertical stress in the central of the coal pillar was close to the peak stress, and the stress curve of the coal pillar gradually changed from two-peak shapes to the asymmetric trapezoid shape. (3) When the wide coal pillar is located in IV-IV, V–V and, VI-VI (20 m, 100 m, and 180 m behind LW3102, respectively), the

TABLE 3: Discrimination of broken features of key strata.

Key strata	SKS1 (fine sandstone)	SKS2 (coarse sandstone)	SKS3 (siltstone)
Overhanging width (m)	288	264	171
Weighting step (m)	29	58	190
Overhanging area (m^2)	8352	15312	32490
Broken features	Perpendicular "O-X" Near-field key strata	Perpendicular "O-X" Near-field key strata	Parallel "O-X" Far-field key strata

TABLE 4: Physical and mechanical parameters of coal and rock.

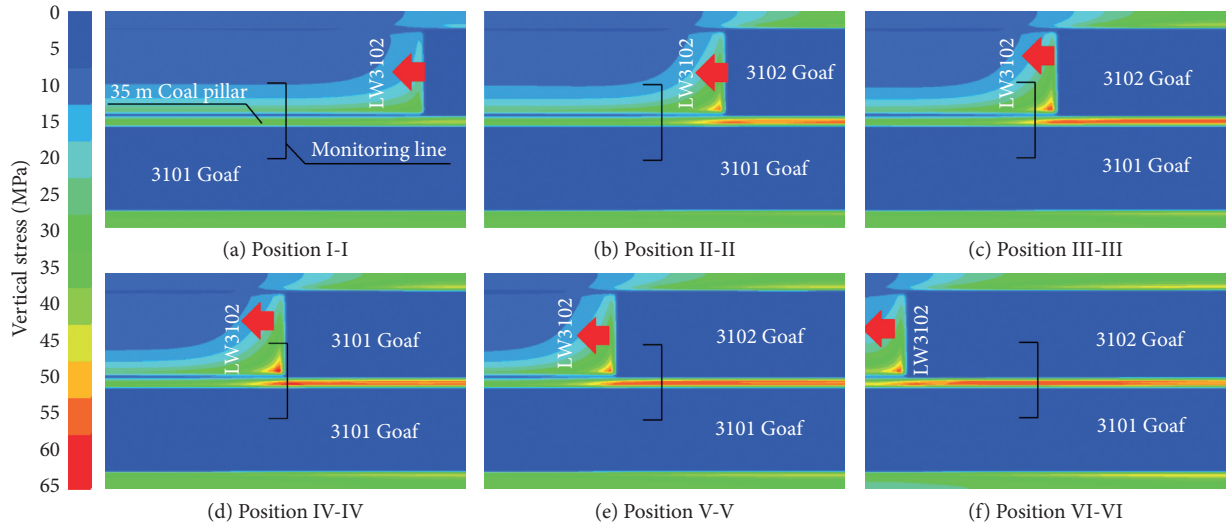| Lithology	Density (kg/m^3)	Bulk modulus (GPa)	Shear modulus (GPa)	Friction angle (°)	Tensile strength (MPa)
Coal	1832	1.25	1.3	42.02	1.77
Sandy mudstone	2321	4.04	3.03	26.10	4.34
Medium sandstone	2294	4.76	2.99	27.23	3.32
Coarse sandstone	2343	5.38	3.54	31.53	4.13
Fine sandstone	2352	13.63	4.88	30.82	5.67
Silstone	2355	4.17	2.63	21.31	3.62

FIGURE 6: Vertical stress evolution nephogram of 35 m coal pillar. (a) Position I-I. (b) Position II-II. (c) Position III-III. (d) Position IV-IV. (e) Position V-V. (f) Position VI-VI.

surrounding coal pillar changed from single goaf to double goaf and the abutment pressure of both goaves was superimposed. The vertical stress of the coal pillar continued to rise to 53.67 MPa, 58.77 MPa, and 60.39 MPa, respectively. At this time, the vertical stress in the center of the coal pillar reached the peak stress, and the stress curve of the coal pillar gradually changed from asymmetric trapezoid to symmetrical trapezoid shape.

The occurrence of coal pillar bursts was affected by the stress concentration and the size of the internal burst core [25]. The simulation results showed that the stress distribution of wide coal pillar went through three states: two-peak shapes, asymmetric trapezoid shape, and symmetrical trapezoid shape with the different advancing position of working face, and the maximum stress concentration factors were 1.69, 2.53, and 3.45, respectively. The stress distribution of the coal pillar at position VI-VI was a symmetrical trapezoid, and the vertical stress was the highest, but the internal burst core was the smallest.

Therefore, it was far from the LW3102 when the pillar burst in position VI-VI and had minor disturbance to the working face. On the other hand, the distribution of plastic zone and the size of burst core of coal pillar at positions I–I, II-II, and III-III were similar, but the stress concentration of coal pillar at position III-III was high, which was the closest to the working face. Therefore, it was the highest risk of rock burst of symmetrical trapezoid wide coal pillar at III-III position.

3.3. Analysis of Stress Distribution in Wide Coal Pillar Stope with Multithick Key Strata. Figure 8 shows the coordinate system adopted to determine the stress distribution for wide coal pillar stope with multiple key strata. The static stress in the coal pillar adjacent to the single goaf mainly consists of σ_g (the gravity stress of the surrounding rock), $\Delta\sigma_{gf1}$, and $\Delta\sigma_{gf2}$ (stress increment transferred to the wide coal pillar stope from the overhanging strata in 3101 goaves and goaf of
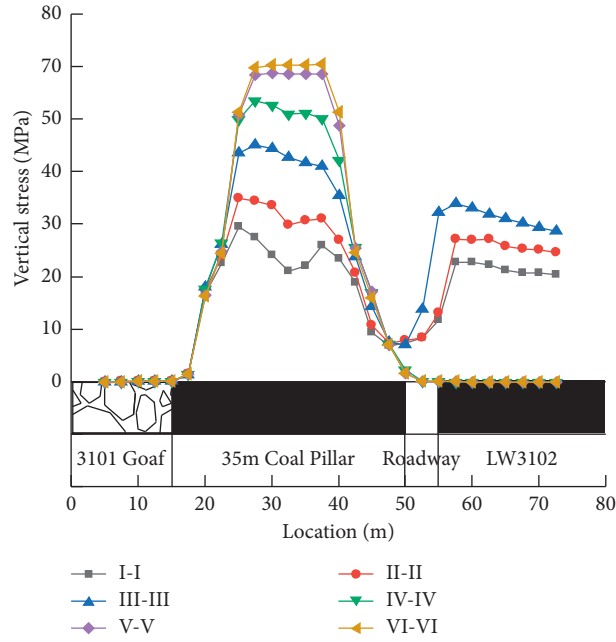
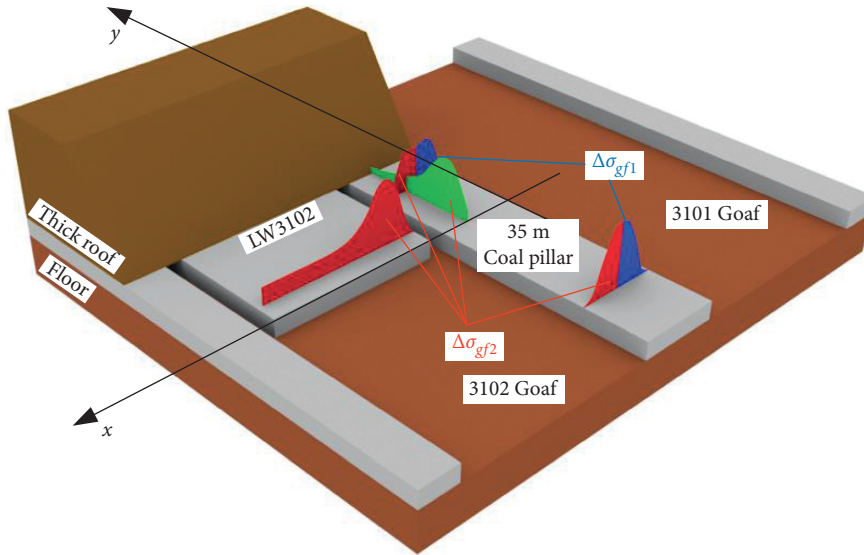FIGURE 7: Vertical stress evolution curve of 35 m coal pillar.

FIGURE 8: Numerical simulated stress distribution of wide pillar stope with multithick key strata.

LW3102) [12]. Therefore, the abutment pressure of the wide pillar stope was expressed by the following equations:

$$\sigma_s = \sigma_g + \Delta\sigma_{gf1} + \Delta\sigma_{gf2}, \tag{5}$$

where the expression for the gravity stress of surrounding rock was

$$\sigma_g = \gamma H. \tag{6}$$

In the previous equation, H is the average buried depth of the working face.

Based on monitoring data, the stress transmitted to the coal seam from each overhanging key strata in the 3101

goaves had a roughly isosceles triangular distribution [26]. Therefore, the stress increment generated by the broken key strata of i was expressed by

$$\Delta\sigma_{gf1} = \begin{cases} \dfrac{\Delta\sigma_{\max} x \tan \alpha}{H_i} & \left(0, \dfrac{H_i}{\tan \alpha}\right) \\[2ex] \Delta\sigma_{\max}\left(2 - \dfrac{x \tan \alpha}{H_i}\right) & \left(\dfrac{H_i}{\tan \alpha}, \dfrac{2H_i}{\tan \alpha}\right), \\[2ex] 0 & \left(\dfrac{2H_i}{\tan \alpha}, +\infty\right) \end{cases} \tag{7}$$

where α is the rock fracture angle, calculated from the ground subsidence data to $65°$ and $\Delta\sigma_{\max}$ is the maximum stress increment generated by broken key strata of i in 3101 goaves on the coal seam around the goaf; the calculation of stress increment $\Delta\sigma_{gf2}$ produced by 3102 goaves was similar.

The equation $\Delta\sigma_{\max}$ was obtained from the stress Q_i transfer from the broken key strata of i in goaf to the coal seam [27]:

$$Q_i = \frac{q_i}{2} = \frac{\gamma L_i (M_i + m_i)}{2},$$

(8)

where q_i is the self-weight of the ith key strata and the overlying strata controlled by it, L_i is the length of the block of broken key strata of i, M_i, and m_i are the thickness of key strata i and the thickness of overlying strata controlled by it, respectively. According to the previous data, the weighting steps for SKS1, SKS2, and SKS3 are 29 m, 58 m, and 190 m, respectively. The thickness of the controlled strata by SKS1, SKS2, and SKS3 is 25.9 m, 99.6 m, and 61.6 m, respectively.

Combining (5)–(8), the expression for the stress distribution in wide coal pillar stope with multithick key strata was derived as given in

$$\sigma_s = \begin{cases} \gamma H + \dfrac{\Delta\sigma_{\max}(x+y)\tan\alpha}{H}, & 0 \leq x, y, \dfrac{H}{\tan\alpha} \\[2mm] \gamma H + \Delta\sigma_{\max}\left(4 - \dfrac{(x+y)\tan\alpha}{H}\right), & \dfrac{H}{\tan\alpha} \leq x, y, \dfrac{2H}{\tan\alpha}. \\[2mm] \gamma H, & \dfrac{2H}{\tan\alpha} \leq x, y \end{cases}$$

(9)

The analysis of Section 2.2 and (9) showed that the rock burst risk of wide coal pillar stope with multikey layer was related to mining depth H, key strata height H_i, and rock fracture angle α. There were three stress concentrations in LW3102, as shown in Figure 8. The advanced region of LW3102 was mainly affected by abutment pressure of 3102 goaves, and the maximum vertical stress was 23.51 MPa by theoretical calculation; under the superposition of abutment pressure of overhanging strata in 3101 goaves and goaf of LW3102, the stress distribution of coal pillar located in the advanced region and goaf of LW3102 are asymmetric trapezoid shape and symmetrical trapezoid shape, respectively, and the vertical stress in this area was the largest, which was 24.72 MPa.

3.4. Dynamic Stress and Static Stress Combined Characteristics of Wide Coal Pillar Burst with Multithick Key Strata. Rock burst results from the combined dynamic and static stress [28–30], as shown in Figure 9. When the dynamic stress and static stress of coal and rock mass exceeded the critical stress, rock burst occurred; that is, $\sigma_s + \sigma_d \geq \sigma_{B\min}$, σ_s was static stress in coal and rock mass, σ_d was the dynamic stress-induced by MS events, and $\sigma_{B\min}$ was the critical stress of rock burst.
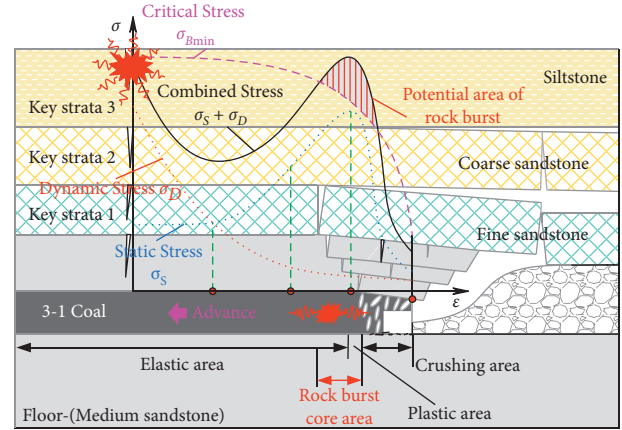

Figure 9: Rock burst mechanism of dynamic stress and static stress combined in wide pillar stope with multithick key strata.

Under the influence of abutment pressure, the coal along the strike direction of the working face was divided into three areas: crushing area, plastic area, and elastic area, and with the increase of distance from the working face, the greater the integrity of coal, the higher the critical stress $\sigma_{B\min}$ of rock burst. The dynamic stress σ_d decreased exponentially with the distance from the MS source, and static stress σ_s was mainly affected by the abutment pressure, and its shape was similar to abutment pressure. Therefore, the combined stress $\sigma_s + \sigma_d$ curve superimposed by dynamic and static stresses showed "ascent-descent-ascent" variations with the distance from the working face. In the plastic area and some elastic areas, the combined stress was higher than the critical stress, the potential area of rock burst.

The SKS3 far-field key strata in LW3102 was characterized by a long breaking distance, large overhanging area, and high energy released, and the stress of wide coal pillar in position III-III was high concentration with symmetrical trapezoid shape. Therefore, when a long periodic weighting occurred, the superposition of the dynamic stress of breaking far-field key stratum and the high static stress in the wide coal pillar at position III-III exceeded its bearing limit, which induced the coal pillar rock burst. Therefore, the rock burst mechanism in LW3102 was that a large amount of energy was released when the extra thick key strata broke, and a large amount of elastic energy accumulated in the wide coal pillar was superimposed. As a result, accumulated energy in the hard roof and coal body is released nonlinearly into the influence area of abutment stress.

4. Analysis on the Evolution of Coal Pillar Burst with Multithick Key Strata

According to the width mechanism of coal pillar burst induced by multithick key strata, coal pillar burst is related to stope stress evolution and key strata activity. This section analyzes the appearance law of rock burst in LW3102 based on the time-series development of MS energy, frequency, and hydraulic support resistance that reflected the direction of key strata activity and the MS events spatial development that demonstrated the stope stress [31].
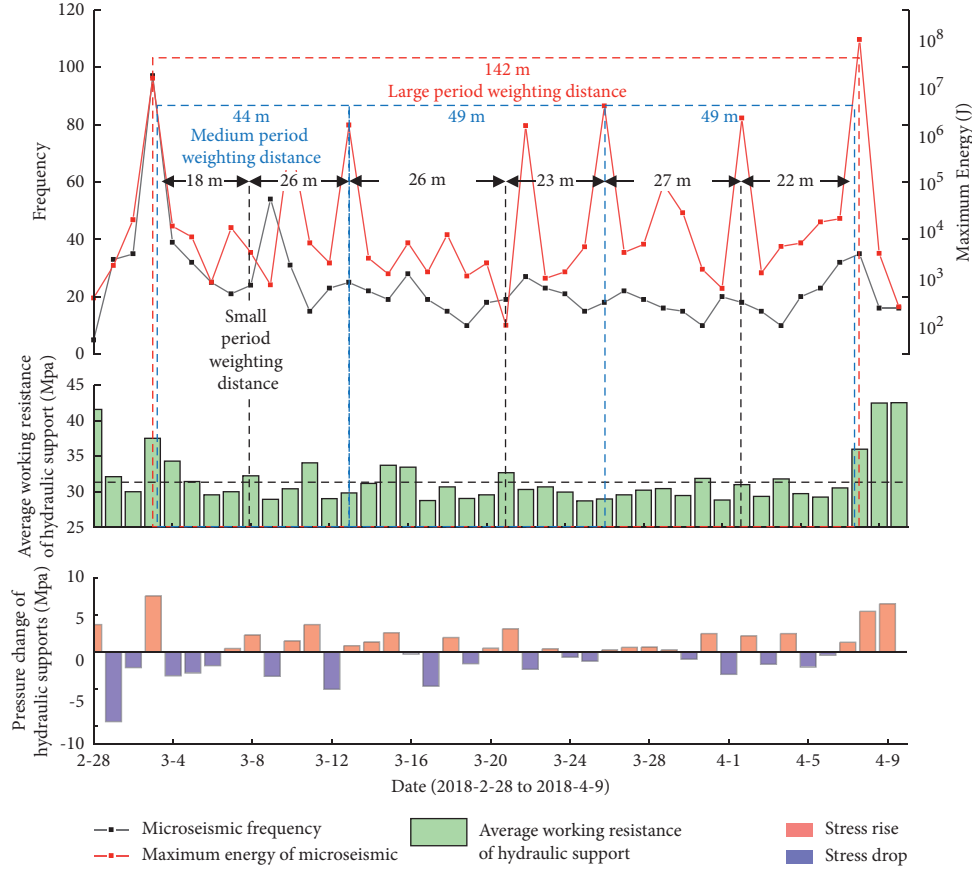
FIGURE 10: Time-series evolution of total energy, frequency of MS events, and hydraulic support stress.

4.1. Time-Series Evolution of MS Energy, Frequency, and Hydraulic Support Stress.

The daily maximum energy and frequency of MS events of LW3102 and the average values of 154 and 172 hydraulic support resistance, which reflected the key strata activity near the wide coal pillar, were collected and analyzed from February 28, 2018, to April 9, 2018, as shown in Figure 10. Figure 10 shows a significant positive correlation between the frequency and energy of MS events, and when the maximum energy and frequency were at a high level, the working resistance of the hydraulic support kept rising.

When the key stratum broke, the overlying strata controlled by it broke simultaneously, accompanied by an increment of MS frequency and energy and hydraulic support stress. According to this, seven periodic weightings of LW3102 were counted, and the statistical results are in Table 5. The 7 MS events in which more than 10^5 J occurred during the statistical period correspond to the periodic weighting. The time of long and medium periodic weighting coincided with the high energy MS events, and the high energy MS events occurred within 0–3 days after the small periodic weighting.

When the weighting step of different key strata was multiple or close multiple, the low-key strata was prone to synchronous breaking due to the infringement and subsidence of high key strata [15]. That is, the synchronous breaking occurs in large, medium, small periodic weighting

or medium and small periodic weighting. Therefore, the seven periodic weightings in Table 5 are further divided into short, medium, and long standard periodic weighting, corresponding to the breaking of SKS1 fine sandstone, SKS2 coarse sandstone, and SKS3 siltstone. During the statistical period, the step of long periodic weighting was 142 m, which induced the "3.3" and "4.8" rock burst, respectively; the measure of regular medium periodic weighting was 44–49 m; the distance of small periodic weighting was 18–27 m, which was consistent with the previous analysis.

As shown in Table 6, SKS3 has the most significant energy released during long periodic weighting due to its longest weighting step, largest breaking area, and the highest increment of hydraulic support stress. The high energy MS

TABLE 5: Breaking and periodic weighting statistics of key strata.

Periodic weighting		The largest MS		Periodic weighting distance (m)		
Date	Type	Date	Energy (J)	Short	Medium	Long
3.3	Long	3.3	6.4×10^6	—	—	—
3.7	Short	3.10	5.6×10^5	18	44	
3.13	Medium	3.13	9.8×10^5	26		
3.20	Short	3.22	9.5×10^5	26	49	142
3.26	Medium	3.26	2.1×10^6	23		
4.2	Short	4.2	1.3×10^6	27	49	
4.8	Long	4.8	3.0×10^7	22		

TABLE 6: Increment of hydraulic support stress and energy of high energy MS events during periodic weighting.

Periodic weighting type	The energy of high energy MS events (J)		Change of hydraulic support stress (MPa)	
	Maximum	Minimum	Maximum	Minimum
Long	3.0×10^7	6.4×10^5	7.55	6.50
Medium	2.1×10^6	9.8×10^5	2.56	0.65
Short	1.3×10^6	5.6×10^5	3.66	0.39

MS events:

○ $\leq 9.9 \times 10E2$ ✦ "3.3" Rock burst

● $1 \times 10E3$-$9.9 \times 10E4$ ✦ "4.8" Rock burst

🔴 $\geq 1 \times 10E5$

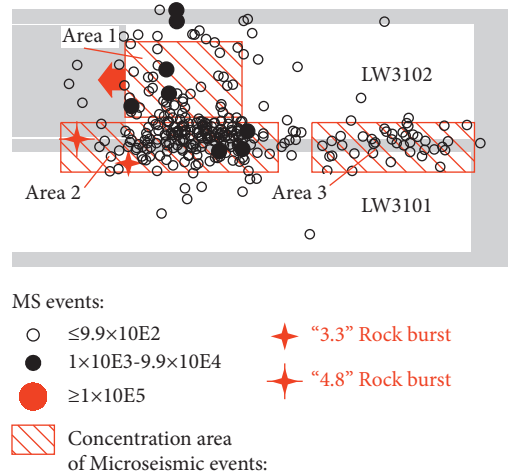▨ Concentration area of Microseismic events:

FIGURE 11: Spatial distribution of MS events in LW3102.

events during long periodic weighting were 6.4×10^6 J to 3.0×10^7 J, 304.8–3061.2%, and 492.3–5357.1% of the medium and short periodic weighting, respectively. The maximum increment of hydraulic support stress was 6.5 MPa to 7.55 MPa, which is 253.9–1161.5% and 177.4–1935.9% of medium and small periodic weighting, respectively.

The statistical results of total energy, frequency of MS events, and hydraulic support stress, combined with the "3.3" and "4.8" rock burst, were closely related to the breaking of key strata. The rock burst risk increased significantly with increased MS frequency, energy, and hydraulic support stress during the periodic weighting. In particular, the MS energy and frequency reached the highest during the long periodic weighting and induced two dynamic disasters ("3.3" and "4.8" rock burst). At this time, the main block of parallel "O-X" SKS3 disturbed the coal pillar stress, and the stress concentration on the coal pillar increased significantly, which was consistent with the hydraulic support stress data.

4.2. Spatial Distribution and Evolution of MS Events. The spatial distribution of MS events was affected by the working face's stress distribution, geological structures, and roof activity [32,33]. As shown in Figure 11, high energy MS events ($\geq 10^3$ J) in LW3102 from January 4 to April 8 occurred over three areas: Area 1 (advanced region of the working face), Area 2 (wide coal pillar ahead of the working face), and Area 3 (wide coal pillar area in goaf), which were

all within the influence range of abutment pressure of goaf, and the stress of coal was high. Not only were the wide coal pillar in Area 2 affected by the abutment pressure superposition of 3102 goaves and 3101 goaves, the vertical stress high, and the distribution nearly asymmetric trapezoid shape, but also they were strongly disturbed by the roof of goaves just after mining, so the distribution of MS events in this area was the most concentrated.

Figures 12 and 13 show the spatial distribution and evolution of MS events before the "4.8" rock burst. During short periodic weighting from April 1 to April 2, SKS1 had intense activity, with MS frequency 37 times, in which the high energy events accounted for 21.6%. The frequency and energy of MS events were high, ranging from 90 m in front of the working face to 260 m behind the working face. From April 3 to April 4, the short periodic weighting ended, the MS frequency was 24 times, in which the high energy events account for 16.7%, and the frequency and energy decreased of MS events significantly, and the distribution area became narrow. From April 5 to April 6, a long periodic weighting would occur, the roofing activity increased, the MS frequency was 42 times, in which the high energy events account for 21.4%, and the distribution area of MS events increased significantly, from 70 m in front of the working face to 520 m behind the working face. From April 7 to April 8, a considerable long periodic weighting occurred. The activity of SKS3 was the strongest, and the frequency and distribution range of MS events were the highest, which were 66 and 760 m, respectively. The maximum energy of a single MS event was 3.0×10^7 J and induced a "4.8" rock burst.
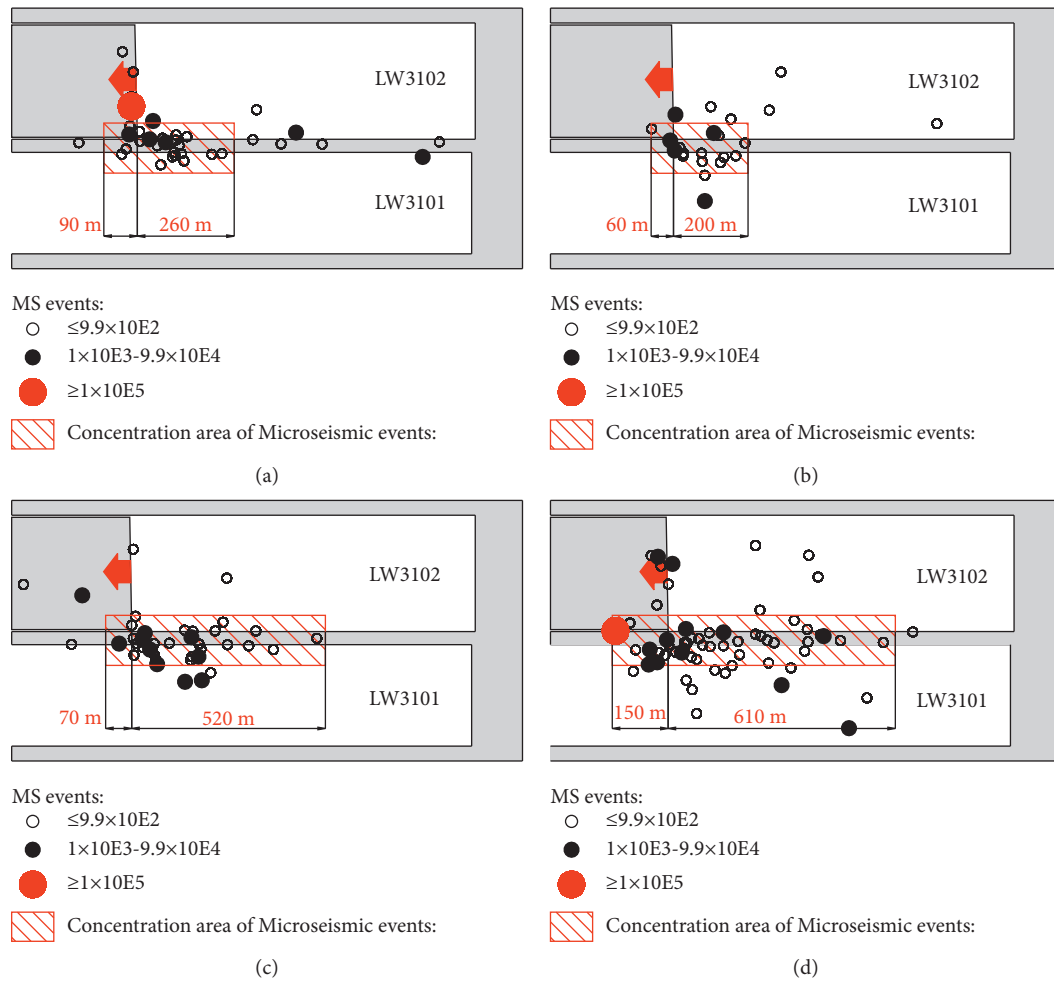
(a)

(b)

(c)

(d)

Figure 12: Spatial distribution of MS events before "4.8" rock burst. (a) Date: April 1 to April 2. (b) Date: April 3 to April 4. (c) Date: April 5 to April 6. (d) Date: April 7 to April 8.
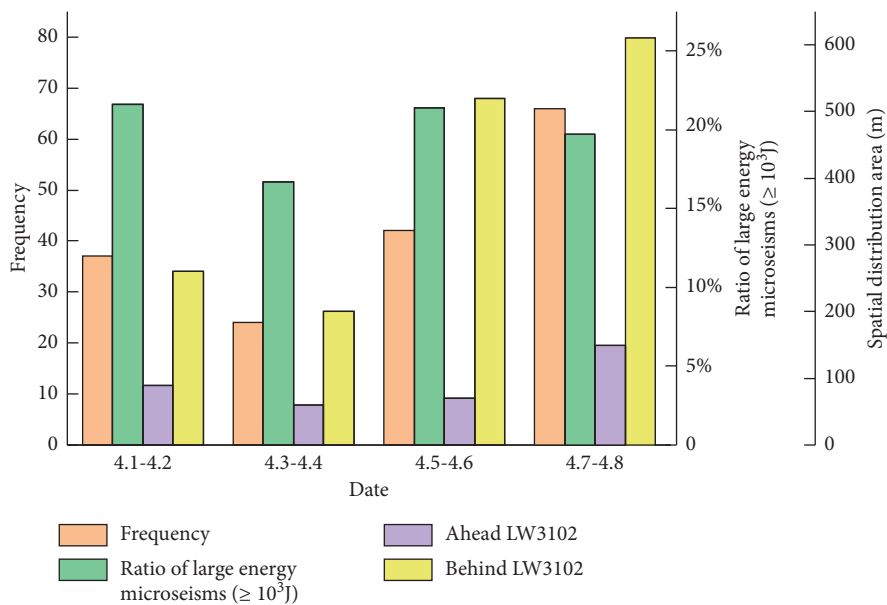

Figure 13: Spatial evolution of MS frequency, energy before "4.8" rock burst.

The analysis of the MS events distribution and evolution showed that the spatial distribution of MS events was three main areas: the advanced area of working face, wide coal pillar area ahead of the working face, and coal pillar in goaf, consistent with the previous inference of LW3102 vertical stress distribution. When periodic weighting of the long, medium, and short occur, the frequency and energy of MS events of LW3102 are enhanced, and the spatial distribution area of MS events increased significantly, which verified that the pillar burst of LW3102 was mainly affected by the vertical stress distribution of coal pillar and key strata activity.

5. Discussion and Conclusion

This research demonstrated that the mechanism of coal pillar bursts induced by multithick key strata was that a large amount of energy released by extra thick key strata broke, and a large amount of elastic energy accumulated in the wide coal pillar was combined, exceeding the critical stress. The energy accumulated in the roof and coal body was then nonlinearly released within the influence range of abutment pressure. Therefore, when the SKS3 broke, the coal pillar burst risk was the highest, and the coal bursting was in the air-return roadway beside the wide coal pillar. Therefore, the prevention of wide coal pillar burst with the multithick key strata included two aspects. On the one hand, hydraulic fracturing or roof presplit blasting shortened the long, medium, and short periodic weighting steps working face. Additionally, it further reduced the overhang area of the key stratum and the energy released during breaking. On the other hand, it changed the coal pillar's width to improve its stress state. For example, it was reducing the width of the coal pillar to reduce the accumulated elastic energy or increasing the width of the coal pillar to make the stress of the coal pillar change from asymmetric trapezoid shape and symmetrical trapezoid shape to two-peak shapes to reduce the stress concentration degree on coal pillar.

The main conclusions from this research were as follows:

(1) The breaking of multithick key strata has the near-field perpendicular "O-X" and far-field parallel "O-X" fracture features. Affected by different breaking characteristics of key strata, such as the weighting step and the energy released, the working face presents three kinds of phenomena in the periodic weighting of the long, medium, and short. The weighting step of the SKS3 key stratum was the longest, the released energy was the highest, and the rock burst risk was the highest.

(2) The 35 m wide coal pillar experienced three stress states: two-peak shapes, asymmetric trapezoid shape, and symmetrical trapezoid shape. In addition, the results of the stope stress analysis showed that the area of the advanced region of working face, wide coal pillar, and the wide coal pillar in goaf have high-stress concentration due to the superposition of abutment stress of goaf.

(3) The time-series evolution of the MS energy, frequency, and stress of hydraulic support showed that the long, medium, and short periodic weighting steps

of multithick key strata were 141.6 m, 43.2–49.6 m, and 17.6–27.2 m, which were consistent with theoretical calculations. In addition, the MS events were distributed around the advanced region of the working face, the wide coal pillar, and the goaf's wide coal pillar, consistent with the analysis results of the high-stress site of the stope.

Data Availability

The figures and tables used to support the findings of this study are included within the article.

Conflicts of Interest

The authors declare no conflicts of interest.

Acknowledgments

References

[1] Q. Zhang, E. Wang, X. Feng, C. Wang, L. Qiu, and H. Wang, "Assessment of rockburst risk in deep mining: an improved comprehensive index method," *Natural Resources Research*, vol. 30, no. 2, pp. 1817–1834, 2021.

[2] T.-B. Zhao, W.-Y. Guo, Y.-L. Tan, Y. C. Yin, L. S. Cai, and J. F. Pan, "Case studies of rock bursts under complicated geological conditions during multi-seam mining at a depth of 800 m," *Rock Mechanics and Rock Engineering*, vol. 51, no. 5, pp. 1539–1564, 2018.

[3] X. Wang, K. Guan, T. Yang, and X. Liu, "Instability mechanism of pillar burst in asymmetric mining based on cusp catastrophe model," *Rock Mechanics and Rock Engineering*, vol. 54, no. 3, pp. 1463–1479, 2021.

[4] A.-y. Cao, L.-m. Dou, C.-b. Wang, X.-x. Yao, J.-y. Dong, and Y. Gu, "Microseismic precursory characteristics of rock burst hazard in mining areas near a large residual coal pillar: a case study from Xuzhuang coal mine, Xuzhou, China," *Rock Mechanics and Rock Engineering*, vol. 49, no. 11, pp. 4407–4422, 2016.

[5] L. Li, W. Li, and Y. Pan, "Influence of impact disturbance on anomalously low friction rock bursts," *Chinese Journal of Rock Mechanics and Engineering*, vol. 38, pp. 111–120, 2019, in chinese.

[6] J. He, L. Dou, S. Gong, J. Li, and Z. Ma, "Rock burst assessment and prediction by dynamic and static stress analysis based on micro-seismic monitoring," *International Journal of Rock Mechanics and Mining Sciences*, vol. 93, pp. 46–53, 2017.

[7] Z.-l. Li, L.-m. Dou, G.-f. Wang, W. Cai, J. He, and Y.-l. Ding, "Risk evaluation of rock burst through theory of static and dynamic stresses superposition," *Journal of Central South University*, vol. 22, no. 2, pp. 676–683, 2015.

[8] H. Maleki, "Coal pillar mechanics of violent failure in U.S. Mines," *International Journal of Mining Science and Technology*, vol. 27, no. 3, pp. 387–392, 2017.

[9] K. Bo-Hyun, W. Gabriel, M. K. Larson, and S. Berry, "Experimental study on the confinement-dependent characteristics of a Utah coal considering the anisotropy by cleats," *International Journal of Rock Mechanics and Mining Sciences*, vol. 105, pp. 182–191, 2018.

[10] Z. Yang, C. Liu, S. Tang, L. Dou, and J. Cao, "Rock burst mechanism analysis in an advanced segment of gob-side entry under different dip angles of the seam and prevention technology," *International Journal of Mining Science and Technology*, vol. 28, no. 6, pp. 891–899, 2018.

[11] C. Newman and D. Newman, "Numerical analysis for the prediction of bump prone conditions: a southern appalachian pillar coal bump case study," *International Conference on Ground Control in Mining*, vol. 31, no. 1, pp. 75–81, 2020.

[12] G. Zhu, L. Dou, A. Cao, and W. Cai, "Assessment and analysis of strata movement with special reference to rock burst mechanism in island longwall panel," *Journal of Central South University*, vol. 12, pp. 209–218, 2017.

[13] Z. Li, L. Dou, W. Cai et al., "Investigation and analysis of the rock burst mechanism induced within fault-pillars," *International Journal of Rock Mechanics and Mining Sciences*, vol. 70, pp. 192–200, 2014.

[14] C.-l. Han, N. Zhang, Z. Ran, R. Gao, and H.-q. Yang, "Superposed disturbance mechanism of sequential overlying strata collapse for gob-side entry retaining and corresponding control strategies," *Journal of Central South University*, vol. 25, no. 9, pp. 2258–2271, 2018.

[15] C. Liu, J. Yang, B. Yu, and F. Wu, "Support resistance determination of fully mechanized top-coal caving face in extra thick seam under multi-layered hard strata," *Journal of Mining and Safety Engineering*, vol. 32, pp. 7–13, 2015, in chinese.

[16] Y. Zhao, J. Zhou, and W. Liu, "Characteristics of ground pressure and mechanism of coal burst in the gob side roadway at Xinjie deep mining area," *Journal of China Coal Society*, vol. 45, pp. 1595–1606, 2020, in chinese.

[17] D. Zhu, S. Tu, H. Tu, and Z. Yang, "Mechanisms of support failure and prevention measures under double-layer room mining gobs – a case study: shigetai coal mine," *International Journal of Mining Science and Technology*, vol. 29, pp. 1595–1606, 2018.

[18] B. Yu, W. Zhu, and R. Gao, "Strata structure and its effect mechanism of large space stope for fullymechanized sublevel caving mining of extremely thick coal seam," *Journal of China Coal Society*, vol. 41, pp. 571–580, 2016, in chinese.

[19] S. Liang, D. Elsworth, X. Li, X. Fu, B. Sun, and Q. Yao, "Key strata characteristics controlling the integrity of deep wells in longwall mining areas," *International Journal of Coal Geology*, vol. 172, pp. 31–42, 2017.

[20] C. Wang, G. Si, C. Zhang, A. Cao, and I. Canbulat, "Location error based seismic cluster analysis and its application to burst damage assessment in underground coal mines," *International Journal of Rock Mechanics and Mining Sciences*, vol. 143, no. 1, Article ID 104784, 2021.

[21] J. Feng, P. Huang, S. Guo, M. Xiao, and L. Lan, "A roof model and its application in solid backfilling mining," *International Journal of Mining Science and Technology*, vol. 27, pp. 139–143, 2017.

[22] C. Wang, A. Cao, G. Zhu, G. Jing, J. Li, and T. Chen, "Mechanism of rock burst induced by fault slip in an island coal panel and hazard assessment using seismic tomography: a case study from Xuzhuang colliery, Xuzhou, China," *Geosciences Journal*, vol. 21, no. 3, pp. 469–481, 2017.

[23] B. Yu, Z. Zhang, T. Kuang, and J. Liu, "Stress changes and deformation monitoring of longwall coal pillars located in weak ground," *Rock Mechanics and Rock Engineering*, vol. 49, no. 8, pp. 3293–3305, 2016.

[24] H. Wang, C. Jiang, P. Zheng, W. Zhao, and N. Li, "A combined supporting system based on filled-wall method for semi

[25] C. Mark and M. Gauna, "Pillar design and coal burst experience in Utah book cliffs longwall operations," *International Journal of Mining Science and Technology*, vol. 31, pp. 33–41, 2020.

[26] Y. Feng, F. Jiang, and J. Li, "Evaluation method of rock burst hazard induced by overall instability of island coal face," *Journal of China Coal Society*, vol. 40, no. 5, pp. 1001–1007, 2015, in chinese.

[27] M. Qian, X. Miao, and J. Xu, "Theoretical study of key stratum in ground control," *Journal of China Coal Society*, vol. 3, pp. 2–7, 1996, in chinese.

[28] J. He, L.-m. Dou, A.-y. Cao, S.-y. Gong, and J.-w. Lü, "Rock burst induced by roof breakage and its prevention," *Journal of Central South University*, vol. 19, no. 4, pp. 1086–1091, 2012.

[29] W. Cai, L. Dou, G. Si et al., "A new seismic-based strain energy methodology for coal burst forecasting in underground coal mines," *International Journal of Rock Mechanics and Mining Sciences*, vol. 123, pp. 86–104, 2019.

[30] W. Cai, L. Dou, G. Si, and Y. Hu, "Fault-induced coal burst mechanism under mining-induced static and dynamic stresses," *Engineering Times*, vol. 7, pp. 687–700, 2020.

[31] C. Wang, G. Si, C. Zhang, and A. Cao, "A statistical method to assess the data integrity and reliability of seismic monitoring systems in underground mines," *Rock Mechanics and Rock Engineering*, vol. 6, pp. 1–17, 2021.

[32] C.-P. Lu, L.-M. Dou, H. Liu, H.-S. Liu, B. Liu, and B.-B. Du, "Case study on microseismic effect of coal and gas outburst process," *International Journal of Rock Mechanics and Mining Sciences*, vol. 53, pp. 101–110, 2012.

[33] G. Si, W. Cai, S. Wang, and X. Li, "Prediction of relatively high-energy seismic events using spatial-temporal parametrisation of mining-induced seismicity," *Rock Mechanics and Rock Engineering*, vol. 53, no. 1–2, 2020.

coal-rock roadways with large deformations," *Tunnelling and Underground Space Technology*, vol. 99, Article ID 103382, 2020.